Manuscript submitted to
AIMS' Journals
Volume **X**, Number **0X**, XX **200X**

Website: http://AIMsciences.org

pp. **X–XX**

AN INVISCID MODEL FOR NONRIGID IMAGE REGISTRATION

Zhao Yi

Department of Computer Science
University of California
Los Angeles, CA 90095, USA

Justin W.L. Wan

David R. Cheriton School of Computer Science
University of Waterloo
Waterloo, ON N2L 6N3, Canada

(Communicated by the associate editor name)

Abstract. We propose an inviscid model for nonrigid image registration in a particle framework, and derive the corresponding nonlinear partial differential equations for computing the spatial transformation. Our idea is to simulate the template image as a set of free particles moving toward the target positions under applied forces. Our model can accommodate both small and large deformations, with sharper edges and clear texture achieved at less computational cost. We demonstrate the performance of our model on a variety of images including 2D and 3D, mono-modal and multi-modal images.

1. **Introduction.** Image registration requires aligning an image pair, the template and the target, with an optimal transformation. In contrast with rigid registration, nonrigid registration allows changes in shape and size. Numerous approaches for nonrigid registration have been developed. For example, the affine transformation model [26], splines [3], and wavelets [1] have all been suggested. These parametric models usually require user-supplied correspondence between labeled landmarks. A disadvantage of the parametric models is that the limited degrees of freedom may not be adequate for complicated registration problems. An alternative approach is to compute the displacement for each of the pixels. Typically a partial differential equation (PDE) needs to be solved (e.g., [2, 13, 33]). These methods directly exploit image intensities to compute the transformation and hence do not require user-supplied landmarks. (We remark, however, that preprocessing of medical images is often necessary to address the issues of inhomogeneity and nonstandardness before registration starts [21].)

Mathematical models for nonrigid registration can be formulated as a minimization problem where the objective function is a sum of two terms (see e.g. [25]). The first term is a similarity measure which computes the differences (or similarities) between the transformed template and target images. A good quality registration

2000 *Mathematics Subject Classification.* Primary: 65D18, 68U10; Secondary: 94A08.

Key words and phrases. Nonrigid registration, particle method, inviscid model, multi-modal, mutual information.

The second author is supported by the Natural Sciences and Engineering Research Council of Canada.

should give a good match with the target. Minimization of the similarity measure alone, however, is a very ill-posed problem. Hence a second term, often known as the regularization term, is added. The PDE-based approach assigns derivatives for the regularization term. For instance, the diffusion and curvature models [25] involve the second and higher derivatives of the solution. More sophisticated PDE models have been proposed that are motivated by physics. Generally speaking, these models interpret the nonrigid transformation as a physical process. The elastic methods, first proposed by Broit [5] and later extended by Bajcsy et al. [2], model the registration process as the deformation of an elastic solid. Various variational forms [7, 12] and efficiency issues have been discussed [15]. Since the deformation energy caused by stress increases proportionally with the strength of the deformation, elastic models are usually used for accommodating small deformations. To overcome this drawback, Christensen et al. [10] proposed another approach which modeled the registration process by the flow of a viscous fluid. Fluid models can allow relatively larger deformations. However, the computational cost can be high [4, 36]. A fast fluid registration using a convolution technique was developed in [4] to address the efficiency issue.

The viscosity term present in the fluid registration model results in a smoothing effect on the transformation. Consequently, the transformed image using the resulting transformation does not look sharp since edges and small details appear smeared. To minimize the "smearing artifact" resulting from fluid viscosity, we propose to use an inviscid model. Instead of regarding the template image as a fluid continuum with viscous interaction, we simulate the deformation process as a set of free particles moving toward the target positions under applied forces. This is similar to the case of an ideal gas [19] where distances between gas molecules are large enough that internal interaction can be safely ignored and each molecule is viewed as a free particle. If the elastic model is analogous to a solid and the fluid model to a liquid, then our model would be analogous to a gas. Comparing the elastic and fluid models, the latter allows larger deformation in the same way that a liquid is more mobile than a solid. Our particle model preserves this large deformation property, and in addition, it allows more local changes. At this point, it is important to note that physically-based methods model the image alignment, rather than the objects in the images, as a physical process. Thus, it is not true that elastic model is only used for images with solid objects, fluid model for images with liquid objects, and our model for images with gaseous objects. These models are generally applicable to a wide range of images.

Based on the physical behavior of particles, we develop a registration technique expressed in a particle framework. To compute the movement of particles, a Lagrangian reference frame is often used. However, the need to track individual particles can become computationally expensive. Assuming there are a sufficiently large number of particles, we can fit an Eulerian reference frame to the particle framework. The resulting partial differential equations are a nonlinear hyperbolic system whose solution describes the spatial transformation between the images to be registered. This system can be numerically solved using finite difference methods.

We note that a particle registration method was studied in [24] in the context of landmark matching using a geodesic interpolating splines technique. In this approach, a number of particles or knotpoints on the template image and those on the target image are pre-selected. A constrained minimization problem is solved to compute the trajectories connecting the corresponding landmark points. Our approach,

however, has much more particles. In fact, each pixel is a particle. Moreover, the destination of each particle is not specified. The destination points are determined by the model equations. See also [23, 34] for details concerning diffeomorphic representations of deformations and the connection with the fluid registration model. Another related approach is based on the optimal mass transport [16], which also does not have a smoothness constraint. It views images as objects with equal mass, and move one mass to another optimally by applying the Monge-Kantorovich theory. This approach has been applied to image registration as well as morphing applications.

The proposed particle registration technique is quite simple and efficient. Since the particle method can be viewed as an inviscid fluid model, the smearing artifact caused by the viscous terms is eliminated and large deformations can be accommodated. Total computational cost is decreased due to the simple form of the underlying model. Our particle registration technique can produce deformed images with more contrast and sharper edges in less time, as we will demonstrate (cf. Section 4). Moreover, the displacement field is allowed to vary only locally, which would be suitable for applications where local changes in displacement field are desired (see e.g. [18]). We have successfully applied the proposed model to align mono- and multi-modality images, yielding fast and accurate registrations.

The rest of the paper is organized as follows. Section 2 contains an overview of the particle registration technique from derivation to formulation. Section 2.1 interprets the particle framework from the variational point of view, and derives the definition of the body force. Section 3 presents a numerical algorithm for solving the consequent PDE system, with a discussion on regularity. Section 4 compares our approach with the fluid approach on a variety of images. Finally, conclusions are given in Section 5.

2. Methodology.

We denote the intensity of the template image by $I_1(\boldsymbol{x})$ and that of the target image by $I_2(\boldsymbol{x})$, where $0 \leq I_1(\boldsymbol{x}), I_2(\boldsymbol{x}) \leq 1$, and $\boldsymbol{x} \in \Omega$ is the image region. The purpose of image registration is to determine a spatial transformation

$$\Phi : \boldsymbol{x} \mapsto \boldsymbol{x} - \boldsymbol{r}(\boldsymbol{x})$$

such that the transformed or deformed template $I_1(\Phi(\boldsymbol{x}))$ is close to the target in a certain sense. Here $r(x)$ is the displacement (or deformation). Physically-based models determine $r(x)$ by modeling the image deformation process as a dynamical physical system.

In addition to mapping $I_1(x)$ to $I_2(x)$, it is desirable that the spatial transformation Φ have additional properties such as smoothness, angle preservation, and rigid body motion preservation. The fluid model, for instance, would compute a transformation that yields a smoothly varying displacement field due to the viscosity term in the PDE. While the smoothness property may be useful and sometimes necessary in some cases, it also tends to diffuse the displacement field. Consider a moving object on a background which does not move. The correct displacement field should be nonzero on the object but then change to zero discontinuously when approaching the background. The fluid model would not be able to obtain the correct displacement field since the nonzero displacements of the object would diffuse into the displacements in the background, making them nonzero.

We need a model which would allow local changes in the displacement field so that it can capture the motion of a moving object without interfering the displacement

field of the stationary parts. Here, we propose a particle registration method based on an inviscid model. This model has the following features:

1. Local motion of the object is allowed;
2. Zero displacement for objects that do not move (e.g. the background);
3. Topological changes in the object are possible, if needed;
4. The resulting transformed template shows sharp edges and high contrast.

We remark that our model would only produce discontinuous displacement fields at where local changes are necessary. In general, it will still yield smoothly varying displacement fields in regions where there are no sudden changes; see the numerical results in Section 4. The situation is similar to gas dynamics where regions away from shocks remain smooth. We refer to the readers [18] for examples where local varying displacement fields are desired. It is beyond the scope of this paper what applications should employ which registration models. Here, we propose a simple and flexible alternative model that allows the displacement field to change locally when desired, which other models (elastic and fluid) cannot provide.

The construction of the particle registration is as follows. We consider the template image as a set of particles carrying intensity information, each with position $\boldsymbol{x}$, velocity $\boldsymbol{u}$, displacement $\boldsymbol{r}$, unit mass, and responding to a body force $\boldsymbol{b}$. The image deformation process is simulated as free particles moving toward the target positions under applied forces. The total number of particles is assumed to be large enough that we can fit Eulerian reference frame [32] to particle simulation. The velocity field $\boldsymbol{u}(\boldsymbol{x}, t)$ and the displacement field $\boldsymbol{r}(\boldsymbol{x}, t)$ are both defined based on final coordinates of particles. A particle currently located at position $\boldsymbol{x}$ at time t originates at position $\boldsymbol{x} - \boldsymbol{r}(\boldsymbol{x}, t)$.

The initial conditions for the particle registration is naturally chosen to be:

$$\boldsymbol{r}(\boldsymbol{x}, 0) = 0, \boldsymbol{u}(\boldsymbol{x}, 0) = 0, \text{for any } \boldsymbol{x} \in \Omega.$$

For the boundary conditions, since the objects to be registered usually lie at the center of the image, we assume the image boundary only contains background information (i.e. black). Hence zero Dirichlet boundary conditions are used for the particle model:

$$\boldsymbol{r}(\boldsymbol{x}, t) = 0, \boldsymbol{u}(\boldsymbol{x}, t) = 0, \text{for any } \boldsymbol{x} \in \partial\Omega \text{ and } t > 0.$$

We note that other boundary conditions, e.g. Neumann, can also be used, if the boundary intensities are not zero.

For any time $t > 0$, the instantaneous state of a particle is governed by Newton's law of motion. If we assume that there is no internal interaction between particles, the conservation of momentum equations can be written as

$$\frac{d\boldsymbol{u}}{dt} - \boldsymbol{b} = 0, \tag{1}$$

where $\boldsymbol{b}$ is the body force applied to that particle and will be defined later by information from the template and the target images. The first term of (1) represents the force of inertia, i.e., unit mass times the acceleration of a particle.

In the Eulerian reference frame, we have the following relationship [32] between total derivatives and partial derivatives with respect to time

$$\frac{d}{dt} = \frac{\partial}{\partial t} + \boldsymbol{u} \cdot \nabla, \tag{2}$$

where ∇ is the gradient operator. Substituting (2) into (1), we obtain the governing equations for particle registration

$$\frac{\partial \boldsymbol{u}}{\partial t} + \boldsymbol{u} \cdot \nabla \boldsymbol{u} - \boldsymbol{b} = 0. \tag{3}$$

Physically, this means that the body force $\boldsymbol{b}$, which acts upon the whole image domain and drives the registration process, is balanced by the inertial force $d\boldsymbol{u}/dt$ caused by the motion of image deformation.

In contrast with fluid registration, equation (3) ignores internal friction and therefore describes an inviscid model. This is similar to the Euler equations commonly used in gas dynamics

$$\rho \left(\frac{\partial \boldsymbol{u}}{\partial t} + \boldsymbol{u} \cdot \nabla \boldsymbol{u} \right) + \nabla p - \boldsymbol{b} = 0, \tag{4}$$

where ρ is the mass density, and p is the isotropic pressure. In the case of unit density and constant pressure, ∇p and ρ are both neglected and (4) is reduced to (3).

Hyperbolic equations such as (4) have the property of allowing shocks (discontinuities) in the solution, which have been shown to be useful for maintaining sharp edges in image denoising [31] and segmentation [6]. It turns out to be useful for image registration problems as well. For example, multi-object registration with very close distances and totally different motions necessitates a transformation which varies rapidly over a very small common area between the objects. Even for single object registration, as mentioned previously, the displacement field experiences a discontinuous change across the object and the background. Hence, as a special case of (4), our model equation (3) should be able to handle such situations.

To track the movement of a particle through time, we need the notion of velocity

$$\boldsymbol{u} = \frac{d\boldsymbol{r}}{dt}, \tag{5}$$

where $\boldsymbol{r}$ is the resulting displacement which describes the offset of current particle to its original position. Using (2), equation (5) can be rewritten as

$$\boldsymbol{u} = \frac{\partial \boldsymbol{r}}{\partial t} + \boldsymbol{u} \cdot \nabla \boldsymbol{r}. \tag{6}$$

With the computed velocity from (3), equation (6) is used to update the current displacement. Thus, particle registration consists of solving (3) and (6). However, there are three unknowns: $\boldsymbol{u}$, $\boldsymbol{r}$, and $\boldsymbol{b}$. To close the PDE system, we need a definition for the body force $\boldsymbol{b}$. This will be derived by interpreting the particle registration problem as a minimization problem.

2.1. **Minimization formulation.** As mentioned in Section 1, nonrigid registration approaches are often formulated as a minimization problem. In this section, we will consider a variational formulation whose Euler-Lagrange equation is closely related to the particle registration model. By considering this Euler-Lagrange equation, the body force is then defined in the next section.

In the variational formulation, the image registration problem is to determine a transformation Φ such that the distance between the deformed template and the target is minimized in some measure $D(\Phi)$. For mono-modal data, we use an L_2

distance measure [8], also called the sum of squared differences, for $D(\Phi)$:

$$D_{SSD}(\Phi) = \int_{\Omega} |I_1(\Phi(\boldsymbol{x})) - I_2(\boldsymbol{x})|^2 \, d\boldsymbol{x}. \tag{7}$$

We seek the transformation Φ which minimizes the distance measure $D_{SSD}(\Phi)$. We often require Φ to have certain desired properties. An additional term, $R(\Phi)$, known as the regularization term, is imposed. Consequently, image registration is formulated as the following minimization problem

$$\min_{\Phi} \ \frac{\alpha}{2} D_{SSD}(\Phi) + \lambda R(\Phi), \tag{8}$$

where λ is a parameter to be discussed in the next section. The constant α is a user-selected parameter. Varying α changes the weight of the L_2 distance measure, and thus influences the final solution of the underlying model. When α is large, the deformed template will be forced to be identical to the target. However, the corresponding registration problem tends to be ill-posed. The choice of an appropriate α is problem dependent. In practice, we determine α by numerical experiment. Since Φ is determined by $\boldsymbol{r}$, (8) can be rewritten as

$$\min_{\boldsymbol{r}} \ \frac{\alpha}{2} D_{SSD}(\boldsymbol{r}) + \lambda R(\boldsymbol{r}).$$

The regularization term $R(\boldsymbol{r})$ specifies additional information about the desired displacement, and is typically selected to be some form of energy. In elastic models [7, 12], $R(\boldsymbol{r})$ is defined as the elastic potential energy, which has the form (in 2D):

$$R(\boldsymbol{r}) = \int_{\Omega} \sum_{i=1}^{2} \sum_{j=1}^{2} \left\{ \frac{\lambda_e}{2} \frac{\partial r_i}{\partial x_i} \frac{\partial r_j}{\partial x_j} + \frac{\mu_e}{4} \left(\frac{\partial r_i}{\partial x_j} + \frac{\partial r_j}{\partial x_i} \right)^2 \right\} d\boldsymbol{x}.$$

Other regularization terms have also been defined for diffusion and curvature models (see e.g. [25]). Instead of using elastic potential for the regularization term as in elastic models, we consider to use a regularization term which is based on kinetic energy:

$$R(\boldsymbol{r}) = \int_{\Omega} \frac{1}{2} \|\boldsymbol{u}(\boldsymbol{x})\|^2 \, d\boldsymbol{x}. \tag{9}$$

The kinetic energy model minimizes the motion of deformation while registering the image pair. The use of a measure of the velocity as a cost function for a time-dependent deformation process is also considered in [17] which describes it as a minimal action term.

Hence, at any time t during registration, the following minimization problem is solved:

$$\min_{\boldsymbol{r}} \int_{\Omega} \frac{\alpha}{2} |I_1(\boldsymbol{x} - \boldsymbol{r}(\boldsymbol{x}, t)) - I_2(\boldsymbol{x})|^2 \, d\boldsymbol{x} + \lambda \int_{\Omega} \frac{1}{2} \|\boldsymbol{u}(\boldsymbol{x}, t)\|^2 \, d\boldsymbol{x}. \tag{10}$$

The distance measure in (10) drives the registration process, while the kinetic energy regularization term tends to resist the motion. More precisely, in the inviscid particle model, the differences of the transformed template and the target image try to move the pixels (or particles) of the template towards the pixels of the target. In the mean time, the kinetic energy regularization term tries to stop the moving particles. The compromise between the two leads to the minimal motion to register the image pair. This idea is similar to the elastic model in which the amount of displacement is constrained by the potential energy regularization term.

It can be shown that the variation of (9) is just the inertial force $d\boldsymbol{u}/dt$. We illustrate this in the 1D case. Since the integrand in (9) is not written explicitly as a functional of the displacement function, we will rewrite it in terms of $\boldsymbol{r}$. As stated in Section 2, the initial velocity is set to zero. Thus, we have

$$\begin{aligned}\frac{1}{2}u^2(x,t) &= \frac{1}{2}u^2(x,t) - \frac{1}{2}u^2(x,0)\\ &= \int_0^t d\left(\frac{1}{2}u^2\right).\end{aligned}$$

Using the chain rule and taking into account that $u = dr/dt$, we obtain

$$\frac{1}{2}u^2(x,t) = \int_0^t \frac{du}{dt}udt = \int_{r(x,0)}^{r(x,t)} \frac{du}{dt}dr. \tag{11}$$

Hence, (9) can be written as

$$R(r) = \int_\Omega K(r)dx, \tag{12}$$

where the functional $K(r)$ is given by (11). The variation of (12) can be calculated by

$$\frac{\delta R(r)}{\delta r} = \frac{\partial K(r)}{\partial r} = \frac{du}{dt}(x,t).$$

Now, taking the variation of the objective functional in (10) with respect to the displacement, $\boldsymbol{r}(\boldsymbol{x},t)$, gives the following PDE

$$\frac{d\boldsymbol{u}(\boldsymbol{x},t)}{dt} - \frac{\alpha}{\lambda}(I_1(\boldsymbol{x}-\boldsymbol{r}(\boldsymbol{x},t)) - I_2(\boldsymbol{x}))\cdot\nabla I_1(\boldsymbol{x}-\boldsymbol{r}(\boldsymbol{x},t)) = 0. \tag{13}$$

2.2. **Body force.** Comparing (13) with (1), we find that the particle dynamic equation is just the Euler-Lagrange equation of (10) where the second term in (13) is the body force $\boldsymbol{b}$ which moves particles from the template I_1 to the target I_2. Thus, the body force can be viewed as the negative variation of the distance measure $D_{SSD}(\boldsymbol{r})$ with respect to the displacement $\boldsymbol{r}$. Motivated by this observation, one suggestion for the body force is

$$\boldsymbol{b}(\boldsymbol{x},t) = \frac{\alpha}{\lambda}(I_1(\boldsymbol{x}-\boldsymbol{r}(\boldsymbol{x},t)) - I_2(\boldsymbol{x}))\nabla I_1(\boldsymbol{x}-\boldsymbol{r}(\boldsymbol{x},t)). \tag{14}$$

There are two terms in (14); one is the difference term $I_1(\boldsymbol{x}-\boldsymbol{r}(\boldsymbol{x},t)) - I_2(\boldsymbol{x})$, and the other is the gradient term $\nabla I_1(\boldsymbol{x}-\boldsymbol{r}(\boldsymbol{x},t))$. For the purpose of registration, the movement of particles should only slow down when the difference term becomes small, which means the magnitude of $\boldsymbol{b}(\boldsymbol{x},t)$ should be determined solely by the difference term. Thus, we simplify the model by choosing $\lambda = \|\nabla I_1(\boldsymbol{x}-\boldsymbol{r}(\boldsymbol{x},t))\|$ which will normalize the gradient term in the body force definition. Hence, equation (14) becomes

$$\boldsymbol{b}(\boldsymbol{x},t) = \alpha(I(\boldsymbol{x},t) - I_2(\boldsymbol{x}))\frac{\nabla I(\boldsymbol{x},t)}{\|\nabla I(\boldsymbol{x},t)\|}, \tag{15}$$

where $I(\boldsymbol{x},t) = I_1(\boldsymbol{x}-\boldsymbol{r}(\boldsymbol{x},t))$ denotes the deformed template at time t.

We note that in the derivation of (13), λ is a parameter independent of $\boldsymbol{r}$. However, in practice, we observe that the value of λ mainly affects the number of iterations to convergence and has minimal effect on the image result. For convenience, we choose λ to normalize $\nabla I(\boldsymbol{x},t)$ in the body force. Mathematically speaking, the resulting particle registration model would not be equivalent to the variational formulation. However, in practice, we observe essentially the same registration results

when λ is a constant and when λ is not. Our choice, however, leads to much fewer number of iterations. After the choice for λ is fixed, we determine the appropriate range of α for fast convergence.

2.3. **Multi-modality.** For multi-modal image registration, the template and target images have very different intensities for corresponding objects or structures. The L_2 distance measure (7) is not preferable. (However, we note that SSD could be applied for motion estimation based registration techniques [27].) A more general statistical measure, known as the "mutual information" [22, 29, 35], is commonly used.

The particle dynamic equations (3), (6) follow in this case as they are independent of the similarity measure. Similar to the mono-modality case, we will determine the body force by considering a minimization problem which combines the mutual information similarity measure with the proposed kinetic regularizer (9):

$$\min_{\boldsymbol{r}} \ -\alpha \mathcal{M}(I_1, I_2, \boldsymbol{r}) + \lambda \int_\Omega \frac{1}{2} \|\boldsymbol{u}(\boldsymbol{x}, t)\|^2 \, d\boldsymbol{x}, \tag{16}$$

where $\mathcal{M}(I_1, I_2, \boldsymbol{r})$ is the mutual information between the transformed image I_1 and image I_2. The displacement $\boldsymbol{r}$ is determined by maximizing the mutual information with minimal kinetic energy.

We follow the same procedure as in the derivation from (10) to (15). Everything follows similarly except for the definition of the body force, which is now the the variation of the mutual information measure with respect to the displacement $\boldsymbol{r}$. This new body force has a similar form as in [11]. Let $p_{\boldsymbol{r}}^{I_1,I_2}(\alpha, \beta)$ be the joint intensity distribution for the deformed template $I_1(\boldsymbol{x}-\boldsymbol{r})$ and the target $I_2(\boldsymbol{x})$. The mutual information expressed in terms of a Kullback-Leibler divergence is given by

$$\mathcal{M}(I_1, I_2, \boldsymbol{r}) \equiv \int_\Omega p_{\boldsymbol{r}}^{I_1,I_2}(\alpha, \beta) \log \frac{p_{\boldsymbol{r}}^{I_1,I_2}(\alpha, \beta)}{p_{\boldsymbol{r}}^{I_1}(\alpha) p^{I_2}(\beta)} \, d\alpha d\beta,$$

where $p_{\boldsymbol{r}}^{I_1}(\alpha)$ and $p^{I_2}(\beta)$ are the marginal intensity distribution for $I_1(\boldsymbol{x} - \boldsymbol{r})$ and $I_2(\boldsymbol{x})$, respectively. Using the Parzen windowing approach, the joint intensity distribution is estimated by

$$p_{\boldsymbol{r}}^{I_1,I_2}(\alpha, \beta) = \frac{1}{|\Omega|} \int_\Omega \Psi(\alpha - I_1(\boldsymbol{x} - \boldsymbol{r}), \beta - I_2(\boldsymbol{x})) d\boldsymbol{x},$$

where $\Psi(\alpha, \beta)$ is a Parzen windowing kernel. Taking the variation of the mutual information function with respect to the displacement $\boldsymbol{r}$, we obtain

$$\frac{\delta \mathcal{M}}{\delta \boldsymbol{r}} = \frac{1}{|\Omega|} [\Psi * \Gamma](I_1(\boldsymbol{x} - \boldsymbol{r}), I_2(\boldsymbol{x})) \nabla I_1(\boldsymbol{x} - \boldsymbol{r}),$$

where $*$ is the convolution operator and

$$\Gamma(\alpha, \beta) = \frac{1}{p_r^{I_1,I_2}(\alpha, \beta)} \frac{\partial p_r^{I_1,I_2}(\alpha, \beta)}{\partial \alpha} - \frac{1}{p_r^{I_1}(\alpha)} \frac{\partial p_r^{I_1}(\alpha)}{\partial \alpha}.$$

Finally, the new body force is given by

$$b(\boldsymbol{x}, t) = \alpha \frac{1}{|\Omega|} [\Psi * \Gamma](I(\boldsymbol{x}, t), I_2(\boldsymbol{x})) \frac{\nabla I(\boldsymbol{x}, t)}{\|\nabla I(\boldsymbol{x}, t)\|},$$

where λ is defined as in (15).

3. **Implementation.** Combining (3), (6), and (15), the particle registration problem requires solving the following PDE system

$$\begin{aligned} \boldsymbol{b}(\boldsymbol{x},t) &= \alpha(I(\boldsymbol{x},t)-I_2(\boldsymbol{x}))\frac{\nabla I(\boldsymbol{x},t)}{\|\nabla I(\boldsymbol{x},t)\|}, \\ \frac{\partial \boldsymbol{u}(\boldsymbol{x},t)}{\partial t} &= \boldsymbol{b}(\boldsymbol{x},t)-\boldsymbol{u}(\boldsymbol{x},t)\cdot\nabla\boldsymbol{u}(\boldsymbol{x},t), \\ \frac{\partial \boldsymbol{r}(\boldsymbol{x},t)}{\partial t} &= \boldsymbol{u}(\boldsymbol{x},t)-\boldsymbol{u}(\boldsymbol{x},t)\cdot\nabla\boldsymbol{r}(\boldsymbol{x},t). \end{aligned}$$

Note the nonlinearity introduced by the body force and the kinematic derivatives. We numerically solve these equations using finite difference methods.

We note that the gradient operator is sensitive to noise in the image. Thus the deformed template is convolved with a Gaussian kernel prior to the gradient computation. Let G_σ denote the Gaussian kernel with standard deviation σ. Then (15) becomes

$$\boldsymbol{b}(\boldsymbol{x},t)=\alpha(I(\boldsymbol{x},t)-I_2(\boldsymbol{x}))\frac{\nabla G_\sigma * I(\boldsymbol{x},t)}{\|\nabla G_\sigma * I(\boldsymbol{x},t)\|}. \tag{17}$$

To update the movement of particles through time, we discretize the time domain $[0,T]$ into small intervals $0=t_0<\ldots<t_n<\ldots<t_N=T$ and apply explicit Euler integration over time. The semi-discretization of (17), (3) and (6) gives

$$\begin{aligned} \boldsymbol{b}^n(\boldsymbol{x}) &= \alpha(I^n(\boldsymbol{x})-I_2(\boldsymbol{x}))\frac{\nabla \tilde{I}^n(\boldsymbol{x})}{\|\nabla \tilde{I}^n(\boldsymbol{x})\|}, \\ \boldsymbol{u}^{n+1}(\boldsymbol{x}) &= \boldsymbol{u}^n(\boldsymbol{x})+\Delta t^n(\boldsymbol{b}^n(\boldsymbol{x})-\boldsymbol{u}^n(\boldsymbol{x})\cdot\nabla\boldsymbol{u}^n(\boldsymbol{x})), \\ \boldsymbol{r}^{n+1}(\boldsymbol{x}) &= \boldsymbol{r}^n(\boldsymbol{x})+\Delta t^n(\boldsymbol{u}^{n+1}(\boldsymbol{x})-\boldsymbol{u}^{n+1}(\boldsymbol{x})\cdot\nabla\boldsymbol{r}^n(\boldsymbol{x})), \end{aligned}$$

where

$$\begin{aligned} \boldsymbol{b}^n(\boldsymbol{x}) &: \text{approximation of the body force at time } t_n, \\ \boldsymbol{u}^n(\boldsymbol{x}) &: \text{approximation of the velocity at time } t_n, \\ \boldsymbol{r}^n(\boldsymbol{x}) &: \text{approximation of the displacement at time } t_n, \\ I^n(\boldsymbol{x}) &: \text{approximation of the deformed image at time } t_n, \\ \tilde{I}^n(\boldsymbol{x}) &: \text{approximation of the Gaussian smoothed deformed image at time } t_n, \\ \Delta t^n &: \text{time step size at time } t_n. \end{aligned}$$

To compute the movement of particles through space, we discretize the image domain Ω into small cells with the same grid spacing h in every dimension. The unknowns are defined at the cell centers. We use the following notation in two dimensions:

$$\begin{aligned} (i,j) &: \text{discrete indices in } (x,y) \text{ dimension}, \\ D_x^-/D_y^- &: \text{backward difference operator}, \\ D_x^+/D_y^+ &: \text{forward difference operator}, \\ (b,c) &: \text{body force in } (x,y) \text{ dimension}, \\ (u,v) &: \text{velocity in } (x,y) \text{ dimension}, \\ (r,s) &: \text{displacement in } (x,y) \text{ dimension}. \end{aligned}$$

To enhance the stability of the discrete gradient terms, we apply an upwind difference operator which is defined as (x-dimension):

$$D_x^{up}(\gamma) = \frac{(1+\gamma)D_x^- + (1-\gamma)D_x^+}{2},$$

where γ is either -1, 0 or 1. The upwind difference operator $D_y^{up}(\gamma)$ in the y-dimension can be defined similarly. The fully discrete system is given as follows:

$$\begin{aligned}
b_{ij}^n &= \alpha(I_{ij}^n - I_{2,ij})\frac{D_x^{up}(\gamma_1)\tilde{I}_{ij}^n}{\sqrt{(D_x^{up}(\gamma_1)\tilde{I}_{ij}^n)^2 + (D_y^{up}(\gamma_1)\tilde{I}_{ij}^n)^2}},\\
c_{ij}^n &= \alpha(I_{ij}^n - I_{2,ij})\frac{D_y^{up}(\gamma_1)\tilde{I}_{ij}^n}{\sqrt{(D_x^{up}(\gamma_1)\tilde{I}_{ij}^n)^2 + (D_y^{up}(\gamma_1)\tilde{I}_{ij}^n)^2}},\\
u_{ij}^{n+1} &= u_{ij}^n + \Delta t^n(b_{ij}^n - u_{ij}^n D_x^{up}(\gamma_2)u_{ij}^n - v_{ij}^n D_y^{up}(\gamma_3)u_{ij}^n),\\
v_{ij}^{n+1} &= v_{ij}^n + \Delta t^n(c_{ij}^n - u_{ij}^n D_x^{up}(\gamma_2)v_{ij}^n - v_{ij}^n D_y^{up}(\gamma_3)v_{ij}^n),\\
r_{ij}^{n+1} &= r_{ij}^n + \Delta t^n(u_{ij}^{n+1} - u_{ij}^{n+1} D_x^{up}(\gamma_4)r_{ij}^n - v_{ij}^n D_y^{up}(\gamma_5)r_{ij}^n),\\
s_{ij}^{n+1} &= s_{ij}^n + \Delta t^n(v_{ij}^{n+1} - u_{ij}^{n+1} D_x^{up}(\gamma_4)s_{ij}^n - v_{ij}^n D_y^{up}(\gamma_5)s_{ij}^n),
\end{aligned}$$

where

$$\begin{aligned}
\gamma_1 &= \text{sign}(I_{2,ij} - I_{ij}^n),\\
\gamma_2 &= \text{sign}(u_{ij}^n),\\
\gamma_3 &= \text{sign}(v_{ij}^n),\\
\gamma_4 &= \text{sign}(u_{ij}^{n+1}),\\
\gamma_5 &= \text{sign}(v_{ij}^{n+1}).
\end{aligned}$$

We remark that solving the particle registration equations is much more efficient than solving the elastic and fluid model equations where a linear system needs to be solved at each iteration.

The discretization above can be easily extended to 3D. We note that the numerical scheme is first order accurate in time and space. Higher order methods such as Runge-Kutta for the time discretization and total variation diminishing (TVD) schemes for the spatial discretization can also be used. In our experience, we find that our numerical method produces very acceptable registration results. There is essentially no visible difference between the deformed template image and the target image. Consequently, we will not consider higher order methods here and refer the interested readers to [20].

To ensure the stability of numerical computation, we impose the Courant-Friedrichs-Lewy (CFL) conditions [28] which read as follows

$$|u_{\max}|\Delta t < h,\ |v_{\max}|\Delta t < h.$$

Here $|u_{\max}|, |v_{\max}|$ refer to the maximum absolute values of the velocity component in each dimension. In our implementation, we select an adaptive control which satisfies

$$\Delta t = \beta \min\left(\frac{h}{|u_{\max}|}, \frac{h}{|v_{\max}|}\right),$$

where $0 < \beta < 1$ is a safety factor.

To ensure a regular transformation, we keep track of the Jacobian determinant through time

$$J(\boldsymbol{x}, t) = \det(\boldsymbol{I} - \nabla \boldsymbol{r}(\boldsymbol{x}, t)),$$

where $\boldsymbol{I}$ is the identity function. Whenever its minimum value over the grid falls below a certain threshold δ, a regridding procedure is performed to avoid local singularity [9]. We pause the computation and generate a propagated template equal to the current deformed template. The registration process is restarted by using the propagated template as the new template. The initial displacement is reset to zero and the velocity remains the same.

The complete algorithm for particle registration is given in Algorithm 1. This Algorithm will terminate if either the maximum timestep is reached or the deformed template converges to the target.

Algorithm 1: Particle Registration
01. Initialize $n \leftarrow 0$, $(u_{ij}^0, v_{ij}^0) \leftarrow 0$, and $(r_{ij}^0, s_{ij}^0) \leftarrow 0$
02. While n has not reached the maximum number of iterations N
03. Generate the corresponding deformed image I_{ij}^n
04. If $\max_{ij} \lvert I_{ij}^n - I_{2,ij} \rvert$ is less than some stopping criteria ϵ
05. STOP
06. EndIf
07. Calculate the applied body force (b_{ij}^n, c_{ij}^n)
08. Compute the instantaneous velocity $(u_{ij}^{n+1}, v_{ij}^{n+1})$
09. Update the current displacement $(r_{ij}^{n+1}, s_{ij}^{n+1})$
10. Track the resultant Jacobian determinant J_{ij}^{n+1}
11. If $\min_{ij} J_{ij}^{n+1}$ is less than a certain threshold δ
12. REGRID
13. EndIf
14. Choose the next step size Δt_n
15. $n \leftarrow n + 1$
16. EndWhile

4. **Numerical Results.** The proposed model is implemented in C and executed on a desktop PC with Intel Core 2 2.13GHz CPU having 3062MB memory. The tunable parameters are typically set to $N = 250$, $\epsilon = 0.01$, $\alpha = 100$, $\delta = 0.5$, $\beta = 0.5$. As a reference, we also implemented the original fluid approach [10] and the known fast acceleration version [4] with viscosity coefficients $\mu = 1$, $\lambda = 0$ (standard values in the literature). As illustrated in [10], elastic models cannot capture large variations from the template to the target. So, we shall compare the particle model with the fluid approach only.

We demonstrate the effectiveness of the proposed model by six examples. The first five are mono-modal registrations in 2D and 3D. The last one is a 2D multi-modal registration. We assume in all the experiments that the objects of interest are originally overlapped in the image pair. This requirement can be easily satisfied by a simple initial alignment. The intensity values are normalized into the range of $[0, 1]$ before registration is performed.

Examples 3-6 have noise in the images. For the typical noise level in the images we have tried, we do not observe any significant effect caused by the noise. We have not tried images with very high noise level, but it is anticipated that high noise levels would in general affect the registration quality and that the iterative process would more likely to converge to a local minimum.

4.1. **Example 1.** We demonstrate the ability of our model to accommodate large curved deformations, as the fluid model does. The target image is the letter "C" and the template image is a small patch of it; see Fig. 1. The same example images are used by the fluid model in [10].

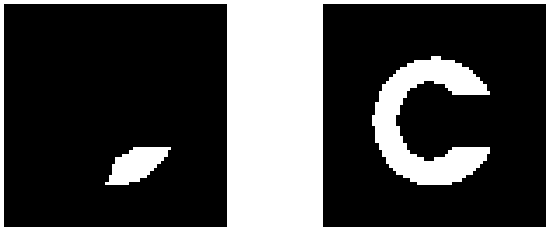

FIGURE 1. Example images from [10]. (Left) template, (right) target.

Fig. 2 shows the progress of deforming a small patch to a longer curved "C" using the particle registration model. The images from left to right are the propagated templates in a forward time series. We can see that our model allows the patch template to grow into the "C" target, with the upside of "C" filled by the dilation of the patch. Eventually, the image pair is matched completely.

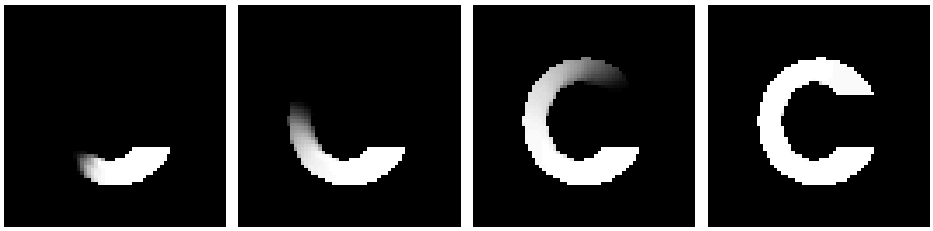

FIGURE 2. Deformation progress from the patch template to the "C" target.

We note that the deformation of this example is uncommonly large compared to most image registrations in practice. It is mainly for illustration only. Usually, a rigid registration is performed before applying nonrigid registration. Hence, one seldom needs register images with excessive large deformation.

4.2. **Example 2.** We compare the fluid and particle models by registering an image of a square to an image of a circle, as shown in Fig. 3. Both images are of size 128×128, with a three-layer nested region at the center. The lengths of the inner, middle, and outer squares are 32, 52, and 72 pixels, while the diameters of the inner, middle, and outer circles are 40, 60, and 80 pixels.

Fig. 4 shows the registration results given by the particle model. The deformed template (left) is a visual assessment of the registration accuracy. It matches exactly

FIGURE 3. (Left) template image of a square, (right) target image of a circle.

with the nested shape of the circle target. The difference image between the template and the target (middle) is an estimation of variability before registration. The intensity differences of the two images are normalized to the range $[-1, 1]$ such that positive differences are indicated by while, negative differences by black, and zero differences by grey. Since the difference image between the deformed template and the target (right) is totally grey (no differences), the deformed template matches completely with the target. The registration results given by the fluid model in this case are similar and we do not provide them here.

FIGURE 4. Registration results given by the particle model. (Left) deformed template, (middle) difference image between template and target, (right) difference image between deformed template and target.

While both the particle and fluid models are able to deform the template into the target, the way to deform the image is very different. Fig. 5 compares the displacement fields given by the particle and fluid transformations. The particle transformation mainly takes place at the corner and mid-side regions. These are also the locations where the template and target differ. Naturally, one would deform such regions to match the template and target while leaving the other regions unchanged. The particle transformation does exactly this. Moreover, there is essentially no displacement in the background where no motion occurs. In contrast, the displacements given by the fluid transformation are nonzero everywhere. Since the background has constant intensity 0, the nonzero displacements would not affect the final outcome of the deformed template. Nevertheless, it is counterintuitive that the background shows nonzero movements.

In the inviscid particle model, the pixels or particles are driven by the force vector $\boldsymbol{b}$ as defined in (17). The magnitude of this driving force is proportional to the difference of the transformed image and the target image. For most pixels in the background, they are the same (black) on both template and target images. Thus,

the driving force is zero and hence the particles do not move. For the other pixels of the template, they are moved towards the pixels of the target. The kinetic energy regularization term then stops the moving particles when they approach the target image. In the fluid model, the driving force is defined similarly. The template is also driven towards the target. The registration process is similar to fluid flow and the motion will eventually be slowed down by the "internal friction" modeled by the viscosity term in the fluid registration equation. However, due to the viscosity term, there is a diffusion effect on the displacements. More precisely, if there is nonzero displacement at one pixel, the neighboring pixels will also have nonzero displacements. It explains the phantom motion in the background.

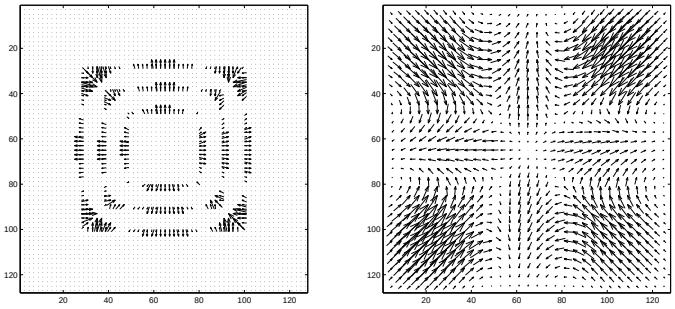

FIGURE 5. Displacement fields produced by (left) the particle model, and (right) fluid model.

4.3. **Example 3.** In this example, we apply the particle and fluid models to register images with topological changes. Fig. 6 shows a template of a white connected region with two squares connected by a line. (One could also view it as a black region with one hole.) The target has two disconnected white squares. (The black region now has two holes.) The registration results are shown in Fig. 7. The particle model is able to register the images by allowing topological changes. By examining the displacement field, it "removes" the white line by covering it with the black background. The fluid model, on the other hand, leaves a thin white line connecting the two squares.

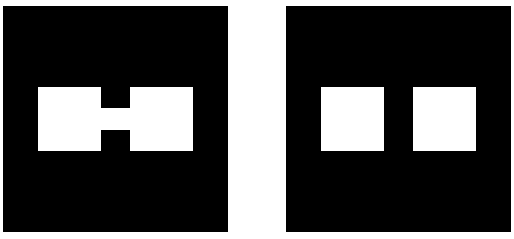

FIGURE 6. (Left) template, (right) target showing a splitting white region.

4.4. **Example 4.** This experiment is to demonstrate that the inviscid model will lead to fewer blurring artifacts compared with the fluid model. The template (left) and the target (right), as shown in Fig. 8, are 256×256, 8-bit, grey-level images

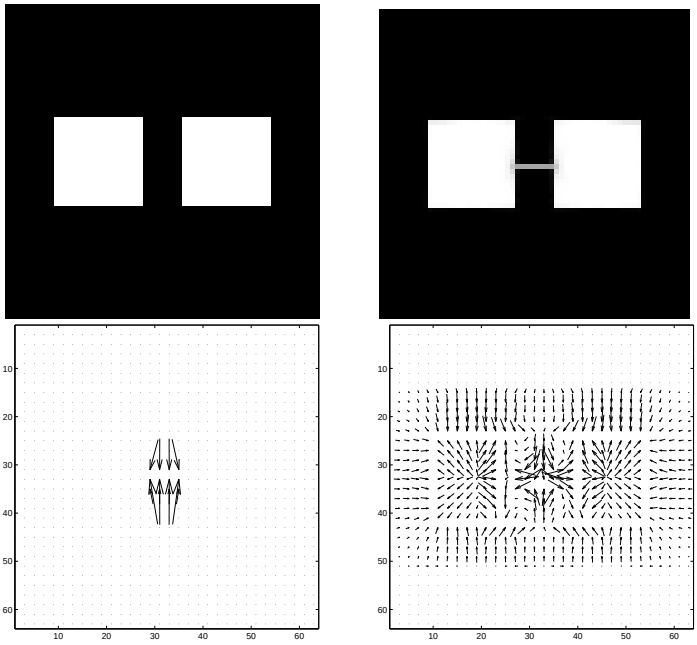

FIGURE 7. Results of registering images with topological changes by (left) particle registration and (right) fluid registration: (top) deformed templates, (bottom) displacement fields.

of segmented brains[1]. The skull part has been stripped and the image pair shows the brain region only. Since these images are slices through different subjects, they exhibit obvious variation from each other in limbic system and internal structures. Hence nonrigid deformation is required to register the image pair.

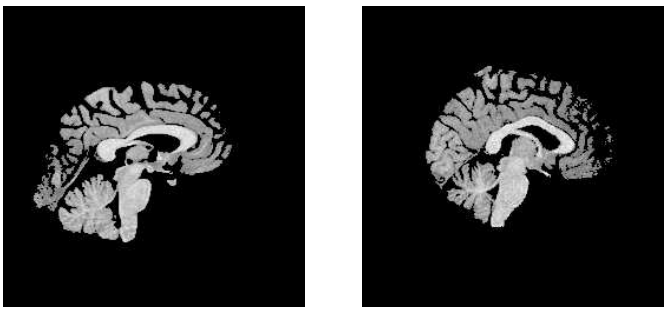

FIGURE 8. (Left) template, (right) target images of segmented brains.

Fig. 9 compares the results given by the particle registration (top) and the fluid registration (bottom). Three sets of images are presented for each registration: the deformed templates (left), the difference images between deformed templates and target (middle), and the displacement fields (right). By inspecting the deformed

[1]These images were provided by the courtesy of H. Farid, Computer Science Department, the Dartmouth College.

templates of the two registrations, we find that the fluid approach leads to a deformed template with blurring in grey cerebral cortex and smearing on the white corpus callosum, while the particle approach allows different structures to move separately and hence avoids such problems. Moreover, the difference image given by the particle model shows less structures of the brain, indicating more accurate overall registration. Also, notice the large displacement field of the background produced by the fluid model due to registering the lower left portion of the brain image.

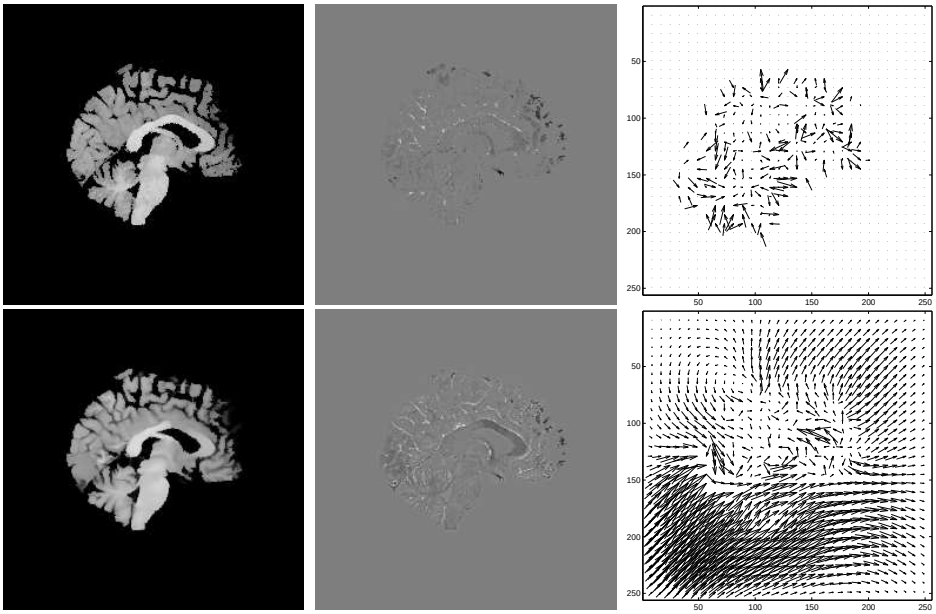

FIGURE 9. Registration results of segmented brains given by (top) the particle model, and (bottom) the fluid model. (Left) deformed templates, (middle) difference images between deformed templates and target, (right) displacement fields.

To better demonstrate that the particle approach yields a deformed template with sharper edges and clearer texture than the fluid approach, we apply a Sobel edge detector [14] on the target and the two deformed templates. As shown in Fig. 10, the edge maps contain intensity values within the interval $[0, 1]$ with sharper edges indicated by higher brightness. The edge map of the particle deformed template is generally brighter than that of the fluid deformed template. Moreover, the small circle features inside the cortical region are preserved by the particle registration, whereas the fluid registration smears the texture and blurs the edges.

4.5. **Example 5.** We show that the proposed model can be extended to accommodate 3D deformations. The MR volumes used here are stacks of segmented coronals through different subjects which are randomly chosen from IBSR[2]. The skull parts have been stripped and the volumes show the brain region only. The template and target are 8-bit, grey-level volumes with a dimension of $256 \times 256 \times 63$

[2]Internet Brain Segmentation Repository. http://www.cma.mgh.harvard.edu/ibsr/

FIGURE 10. Edge maps of (left) target, (middle) particle deformed template, and (right) fluid deformed template.

at $1mm \times 1mm \times 3mm$. They are symmetrically padded by zeros to produce $256 \times 256 \times 80$ full resolution so that Dirichlet boundary conditions can be used. Since the borders of the $x - y$ planes are mostly black, registration is performed in the central square region only, and the final grid size is chosen to be $160 \times 160 \times 80$.

A coarse-to-fine multiresolution scheme is used to speed up computation. We first focus on the global motion pattern at a coarse level of the image. The fine target and template images are downsampled to coarse images. Thus, each pixel of the coarse image is formed by agglomerating 2×2 pixels of the fine image. The coarse intensity is given by the average of the corresponding fine intensities. The particle registration is then performed on the downsampled images. Afterwards, the coarse deformed template and the coarse displacement field are upsampled to the fine level by linear interpolation. They are used as an initial guess for the fine level registration. Then we refine the results with the details obtained from the finer image. The entire procedure can be repeated for multiple levels. However, in this experiment, a two-level multiresolution is found to be sufficient. Thus the two 3D volumes are downsampled to the coarse level of $80 \times 80 \times 40$.

Fig. 11 shows the 3D registration results. Each row corresponds to a specific coronal slice in the volume (from top to bottom slices 22, 36, 39, 54, and 60, respectively). The columns from left to right correspond to the template, the coarse deformed template, the fine deformed template, and the target, respectively.

4.6. **Example 6.** This example shows a multi-modality image registration using the particle model combined with the mutual information measure. As shown in Fig. 12, the template and target (top) are 200×200, 8-bit, grey-level brain images from MR-TIP[3]. The template (left) is T1-weighted, while the target (right) is T2-weighted. Since they are imaged using different parameters, the intensities are different for corresponding brain structures. The registration results are shown in Fig. 12 (bottom). We can see that particle model successfully deforms the template to the target. For instance, the ventricle has a similar shape as the target. We also show the deformation grid generated by the displacement field. Very minimal deformation is required for aligning the brain structures using the particle model, and there is no deformation in the background.

4.7. **Example 7.** Here, we demonstrate the results of the particle registration and the method based on mass transport, which also does not impose explicitly any

[3]MR Technology Information Portal. http://www.mr-tip.com/

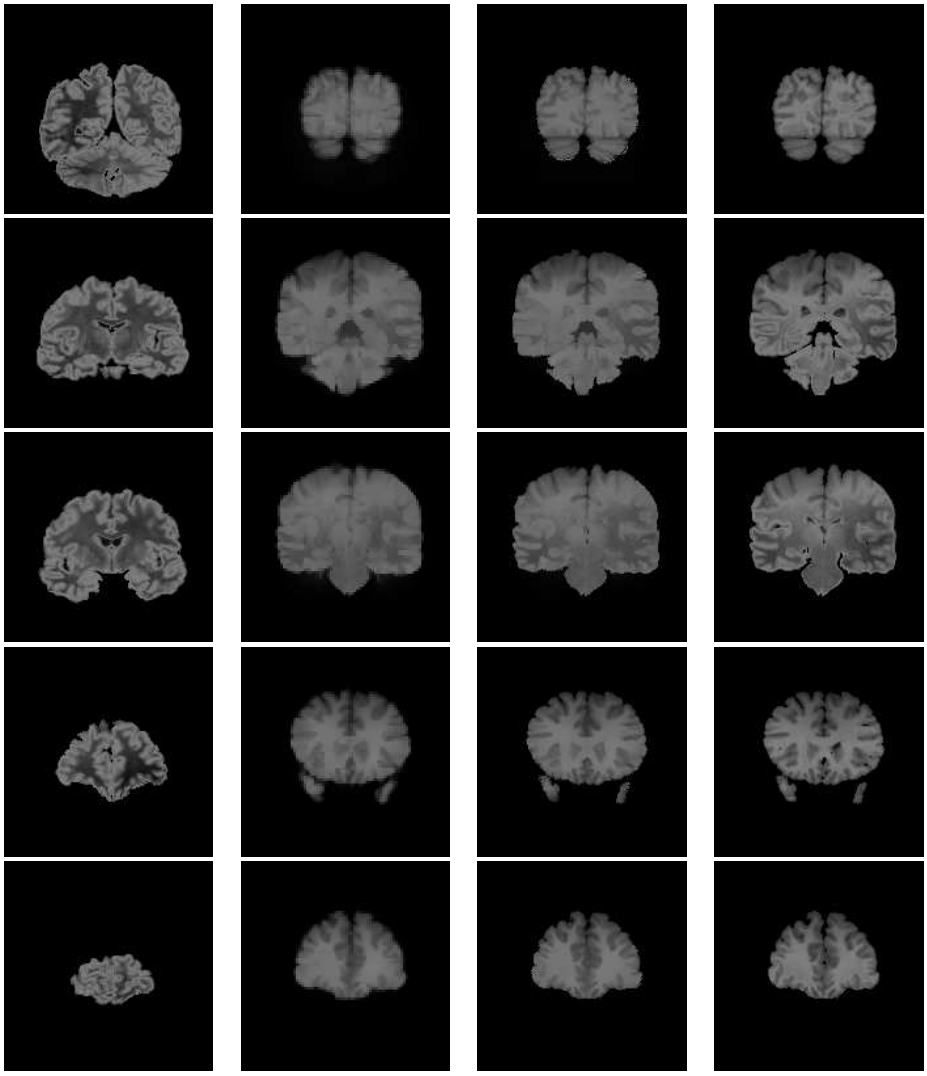

FIGURE 11. 3D registration results given by particle registration. (Left) template, (middle-left) coarse deformed template, (middle-right) fine deformed template, (right) target.

smoothness constraint in the model. We register a pair of 2D Brain MRI images before and during surgery which are used in an example in [30, Fig 6 & 7]. We note that the target and template images used here are not the original images used in [30]; they are frames extracted from an avi file obtained from the authors' website[4]. Thus degradation in image quality may have occurred. The registration results are shown in Fig. 13 (bottom). As in the other examples, the background has very minimal displacement. Compared to the image results in [30], the particle registration result shows slightly more deformation inside the brain, but much less deformation near the top boundary of the brain. Moreover, the the particle model

[4]http://www.bme.gatech.edu/groups/minerva/publications/papers/zhu-extra-index.html

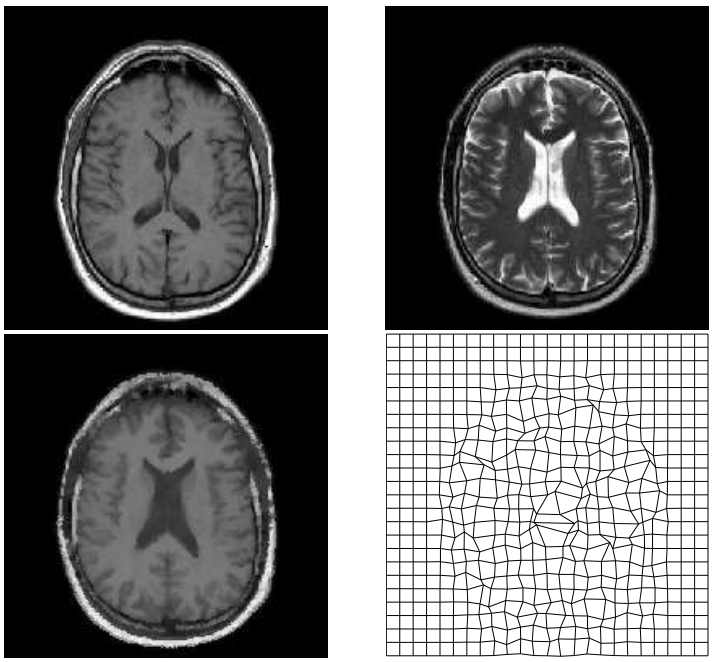

FIGURE 12. Multi-modality image registration results. (Top-left) template, (top-right) target, (bottom-left) deformed template, (bottom-right) deformation grid.

also shows better contrast in the deformed template, especially at the regions of the ventricles and the top left part of the brain.

4.8. **Quantitative Measures.** We show the mean of squared differences (MSD) for the mono-modalilty registration experiments and list them in Table 1. We have also calculated the mean of absolute differences (MAD) and the correlation coefficients (CC). Since the results are qualitatively the same, we do not report them here. For the multi-modality registration experiment (last row), we show the mutual information (MI) values instead. Note that the fluid registration results for the 3D experiment are not provided because the iteration takes too long to converge.

Example	No Registration	Particle Registration	Fast Fluid Registration
1: Patch to "C"	0.103760	0.000045	0.000083
2: Square to Circle	0.010309	0.000002	0.000015
4: Segmented Brain	0.054380	0.001784	0.002936
5: 3D	0.015820	0.000417	—
6: Multi-model	0.786763	1.218577	1.178070

TABLE 1. Mean of squared differences for examples 1, 2, 4, 5 and mutual information values for example 6.

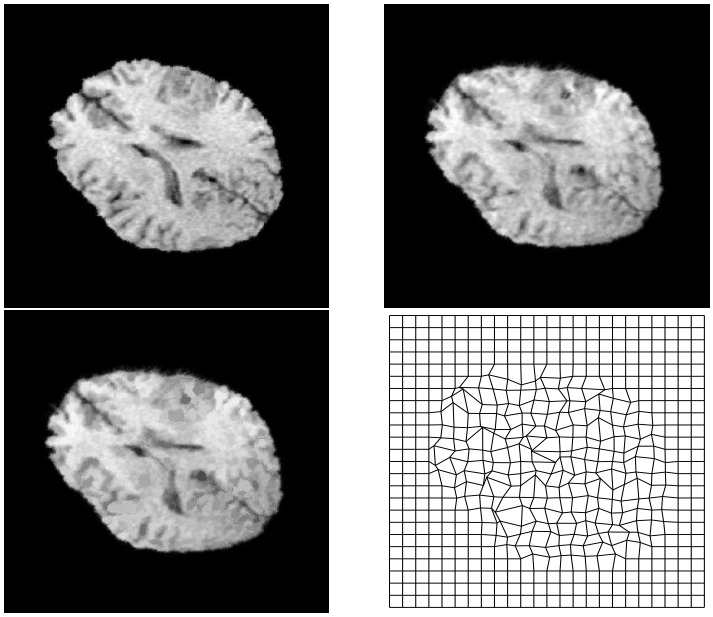

FIGURE 13. Image registration results of a 2D Brain MRI. (Top-left) template, (top-right) target, (bottom-left) deformed template, (bottom-right) deformation grid.

We can see that the MSD after the particle registration are close to zero. We observe the same results for the MAD. (The CC are almost one for all the examples.) It shows that the particle deformed template is quite similar to the target. Comparing with the fluid registration, the particle registration has smaller MSD, (also smaller MAD and bigger CC) which indicates a better registration quality. For the multi-modalilty example 6, the particle registration has larger final mutual information value than the fluid registration does, again showing better registration quality. We do not have a formal proof of why the particle registration performs better in these examples. However, an explanation is that due to the inviscid nature of the particle registration, the smearing artifact is minimal. Thus it is able to produce a transformed template closer to the target, leading to smaller registration errors.

Example	Size	Particle Registration		Fast Fluid Registration	
1: Patch to "C"	64×64	211	0.6s	192	1.2s
2: Square to Circle	128×128	119	1.2s	41	0.84s
4: Segmented Brain	256×256	98	5.3s	159	21.4s
5: 3D	$160 \times 160 \times 80$	121	16.6m	—	—
6: Multi-modal	200×200	179	1.1m	217	3.0m

TABLE 2. Number of iterations and execution times for each experiment

The number of iterations and the execution times for each experiment are summarized in Table 2. We note that each fluid iteration involves much more work

than the particle iteration since the Navier-Lame equations requires solving a linear system in each time step but the Euler's equations do not. Other than example 2, the particle registration generally needs a smaller number of operations and takes less execution times.

5. **Conclusion.** In this paper we present a novel registration technique expressed in a particle framework. This model is an inviscid model designed for nonrigid registration problems. The key features of the proposed model include (1) both small and large deformations can be accommodated, (2) the blurring effect of fluid models is eliminated and deformed images are obtained with sharper edges and clearer texture at less computational cost, and (3) implementation is simple and fast to execute. We have demonstrated the performance of the proposed model on a variety of images including 2D and 3D, mono-modal and multi-modal images. Future effort will be directed towards extension of the model for localized and specialized registration.

REFERENCES

[1] Y. Amit, *A nonlinear variational problem for image matching*, SIAM Scientific Computing, **15** (1994), 207–224.

[2] R. Bajcsy and S. Kovacic, *Multiresolution elastic matching*, Computer Vision, Graphics, and Image Processing, **46** (1989), 1–21.

[3] F.L. Bookstein and W.D.K. Green, *Edge information at landmarks in medical images*, in "Proceedings of Visualization in Biomedical Computing," (1992), 242–258.

[4] M. Bro-Nielsen and C. Gramkow, *Fast fluid registration of medical images*, in "Proceedings of Visualization in Biomedical Computing," (1996), 267–276.

[5] C. Broit, "Optimal registration of deformed images," Ph.D. thesis, University of Pennsylvania, 1981.

[6] T.F. Chan and L.A. Vese, *Active contours without edges*, IEEE Transactions on Image Processing, **10** (2001), 266–277.

[7] G.E. Christensen, S.C. Joshi, and M.I. Miller, *Volumetric transformation of brain anatomy*, IEEE Transactions on Medical Imaging, **16** (1997), 864–877.

[8] G.E. Christensen, R.D. Rabbitt, and M.I. Miller, *A deformable neuroanatomy textbook based on viscous fluid mechanics*, in "Proceeding of Information Science and Systems," (1993), 211–216.

[9] G.E. Christensen, R.D. Rabbitt, and M.I. Miller, *3D brain mapping using a deformable neuroanatomy*, Physics in Medicine and Biology, **39** (1994), 609–618.

[10] G.E. Christensen, R.D. Rabbitt, and M.I. Miller, *Deformable templates using large deformation kinematics*, IEEE Transactions on Image Processing, **5** (1996), 1435–1447.

[11] E. D'Agostino, F. Maes, D. Vandermeulen, and P. Suetens, *A viscous fluid model for multimodal non-rigid image registration using mutual information*, Medical Image Analysis, **7** (2003), 565–575.

[12] C. Davatzikos, *Spatial transformation and registration of brain images using elastically deformable models*, Computer Vision and Image Understanding, **66** (1997), 207–222.

[13] J.C. Gee, D.R. Haynor, M. Reivich, and R. Bajcsy, *Finite element approach to warping of brain images*, in "SPIE Medical Imaging," (1994), 327–337.

[14] R. Gonzalez and R. Woods, "Digital Image Processing," Addison-Wesley, 1992.

[15] E. Haber and J. Modersitzki, *A multilevel method for image registration*, SIAM J. Sci. Comput., **27** (2006), 1594–1607.

[16] S. Haker, L. Zhu, A. Tannenbaum, and S. Angenent, *Optimal mass transport for registration and warping*, International Journal of Computer Vision, **60** (2004), 225–240.

[17] D.D. Holm, J.T. Ratnanather, A. Trouve, and L. Younes, *Soliton dynamics in computational anatomy*, NeuroImage, **23** (2004), 170–178.

[18] S. Kabus, A. Franz, and B. Fischer, *Variational image registration allowing for discontinuities in the displacement field*, in "Image Processing Based on Partial Differential Equations," (eds. X. Tai, K. Lie, T.F. Chan, and S. Osher), Springer Berlin Heidelberg, 2007.

[19] L.D. Landau and E.M. Lifshitz, "Fluid Mechanics," Pergamon, 1987.

[20] R.J. LeVeque, "Finite Volume Methods for Hyperbolic Problems," Cambridge University Press, 2002.
[21] A. Madabhushi and J.K. Udupa, *Interplay between intensity standardization and inhomogeneity correction in MR image processing*, IEEE Transactions on Medical Imaging, **24** (2005), 561–576.
[22] F. Maes, A. Collington, D. Vandermeulen, G. Marchal, and P. Suetens, *Multimodality image registration by maximization of mutual information*, IEEE Transactions on Medical Imaging, **16** (1997), 187–198.
[23] S. Marsland and C.J. Twining, *Constructing diffeomorphic representations for the groupwise analysis of nonrigid registrations of medical images*, IEEE Transactions on Medical Imaging, **23** (2004), 1006–1020.
[24] A. Mills, S. Marsland, and T. Shardlow, *Computing the geodesic interpolating spline*, in "Lecture Notes in Computer Science, volume 4057," (eds. J. Pluim, B. Likar, and F.A. Gerritsen), Springer, (2006), 169–177.
[25] J. Modersitzki, "Numerical Methods for Image Registration," Oxford University Press, Oxford, 2004.
[26] C.A. Pelizzari, G.T.Y. Chen, D.R. Spelbring, R.R. Weichselbaum and C.T. Chen, *Accurate three-dimensional registration of CT, PET, and/or MR images of the brain*, Computer Assisted Tomography, **13** (1989), 20–26.
[27] S. Periaswamy and H. Farid, *Elastic registration in the presence of intensity variations*, IEEE Transactions on Medical Imaging, **22** (2003), 865–874.
[28] R. Peyret and T. Taylor, "Computational Methods for Fluid Flow," Springer, 1983.
[29] J.P.W. Pluim, J.B.A. Maintz, and M.A. Viegever, *Mutual information based registration of medical images: a survey*, IEEE Transactions on Medical Imaging, **22** (2003), 986–1004.
[30] T. Rehman and A. Tannenbaum, *Multigrid optimal mass transport for image registration and morphing*, in "SPIE Conference on Computational Imaging V," 2007.
[31] L.I. Rudin, S. Osher, and E. Fatemi, *Nonlinear total variation based noise removal algorithms*, Physica D, **60** (1992), 259–268.
[32] R. Temam and A. Miranville, "Mathematical Modeling in Continuum Mechanics," Cambridge, 2000.
[33] J. Thirion, *Image matching as a diffusion process: an analogy with Maxwell's demons*, Medical Image Analysis, **2** (1998), 243–260.
[34] A. Trouve, *Diffeomorphisms groups and pattern matching in image analysis*, International Journal of Computer Vision, **28** (1998), 213–221.
[35] P. Viola and W.M. Wells, *Alignment by maximization of mutual information*, International Journal of Computer Vision, **24** (1997), 137–154.
[36] G. Wollny and F. Kruggel, *Computational cost of nonrigid registration algorithms based on fluid dynamics*, IEEE Transactions on Medical Imaging, **21** (2002), 946–952.

Received xxxx 20xx; revised xxxx 20xx.

E-mail address: zyi@ucla.edu
E-mail address: jwlwan@uwaterloo.ca